

Combustion for aerospace propulsion

Use of Faraday instabilities to enhance fuel pulverisation in air-blast atomisers

Madjid Boukra^{a,*}, Alain Cartellier^b, Éric Ducasse^c, Pierre Gajan^a, Marie Lalo^a,
Thomas Noel^d, Alain Strzelecki^a

^a ONERA-DMAE, 2, avenue Edouard-Belin, 31055 Toulouse cedex, France

^b LEGI-CNRS-UJF-INP3, Grenoble, France

^c LMP, Bordeaux, France

^d SNECMA, Villaroche, France

Available online 23 July 2009

Abstract

The atomization of liquids into a spray is an important process in many industrial applications and particularly in the aero-engine sector. Conventional air-blast injectors in aircraft engines today use aerodynamic shearing effects to atomize the liquid fuel. However, at operating conditions where the air velocity is below 30 m/s (such as ground start and high altitude restart) the atomization quality is poor. Consequently combustion is less efficient with high pollutant emissions. The objective of this study is to validate a new concept of injector which couples the shearing effects with the principle of ultrasonic atomization. The latter consists of using piezoelectric actuators to generate the oscillations of a wall in contact with the liquid film. This excitation perpendicular to the liquid film surface creates Faraday instabilities at the liquid/air interface. Amplitudes higher than a defined threshold value induce the break-up of ligaments and the formation of droplets. **To cite this article: M. Boukra et al., C. R. Mecanique 337 (2009).** © 2009 Académie des sciences. Published by Elsevier Masson SAS. All rights reserved.

Résumé

Application de méthodes actives pour l'amélioration de la pulvérisation dans un injecteur aérodynamique. La pulvérisation de liquide représente un processus utilisé dans de nombreuses applications industrielles et en particulier dans le domaine des moteurs aéronautiques. Les injecteurs aérodynamiques des turboréacteurs actuels utilisent le cisaillement d'air pour atomiser le carburant liquide. Cependant, dans certaines conditions telles que le ré-allumage en haute altitude, la vitesse de l'air, la pression et la température sont trop faibles pour permettre une bonne pulvérisation. L'objectif de cette recherche est de valider un nouveau concept d'injecteurs couplant les effets de cisaillement aérodynamique avec l'atomisation ultrasonique. Des actionneurs piézoélectriques génèrent l'oscillation d'une paroi en contact avec le film liquide. Cette excitation perpendiculaire à l'interface liquide/air crée des instabilités de Faraday à la surface du film. Des amplitudes d'excitations supérieures à un seuil donné, provoquent la rupture de ligaments et la formation des gouttelettes. **Pour citer cet article : M. Boukra et al., C. R. Mecanique 337 (2009).** © 2009 Académie des sciences. Published by Elsevier Masson SAS. All rights reserved.

Keywords: Ultrasonic atomization; Air-blast injectors; Liquid atomization

Mots-clés : Pulvérisation ultrasonique ; Injecteur aérodynamique ; Atomisation d'un film liquide

* Corresponding author.

E-mail address: Madjid.boukra@onera.fr (M. Boukra).

Nomenclature

b	Longitudinal wave thickness m	δ_ω	Vorticity thickness m
d_{30}	Median particle diameter m	λ	Wavelength m
D_{32}	Sauter mean diameter m	λ_L	Longitudinal wavelength m
f	Excitation frequency Hz	M	Momentum flux ratio –
g	Acceleration due to gravity m ² /s	λ_T	transverse wavelength m
h	Liquid film thickness m	μ	Liquid viscosity kg/m s
H_g	Height of the gas section m	ρ	Liquid density kg/m ³
V	Flow speed m/s	σ	Surface tension kg/s ²
V_c	Convective speed m/s	a_c	Threshold acceleration m ² /s
g	Subscript referring to gas phase	l	Subscript referring to liquid phase

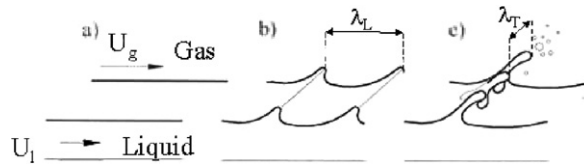


Fig. 1. Primary break-up mechanisms.

1. Introduction

In air-blast injectors, liquid fuel is first spread into a thin annular wall liquid film on a prefilming zone and then is exposed to two high speed co-flowing airstreams forming an annular liquid sheet [1]. This high shearing effect causes the disruption of the liquid phase in a spray of fine droplets. The smaller the droplets, the better the mixing process between air and fuel. Thus the efficiency of the combustion and the level of pollutant emissions depend on the ability of the pulverisation to produce very small droplets. However in some conditions such as high-altitude re-ignition, air speed, pressure and temperature are too low to allow a good pulverisation. In this study, we choose to improve the atomisation of air-blast system by the production of Faraday’s instabilities on the liquid film interface taking place on the prefilming zone. In that scope an experimental set-up generating a liquid film on a prefilming area submitted to a strong co-flowing air stream, is built. After characterization of the aerodynamic stream, the breakup of a liquid film into a spray of droplets by shearing forces will be studied. Then, a modification will be added to the prefilming area introducing a new kind of instability: Faraday’s Instabilities. These instabilities will be analyzed and finally the combined effects of a longitudinal acceleration due to aerodynamic forces and of a controlled acceleration normal to the liquid film will be assessed. Characterization of disruptive mechanisms due to aerodynamic forces and the active method using an ultrasonic actuator will be presented.

2. Literature survey

2.1. Shearing atomisation of a liquid film

The primary atomisation of a liquid film flowing on a prefilming area sheared by a co-current gas stream (Fig. 1a) results from two successive mechanisms. The first one, due to Kelvin–Helmholtz instability, generates longitudinal waves at the free surface of the film as illustrated on Fig. 1b. Previous works [2–4] suggest that the most amplified is driven by the vorticity thickness δ_ω as defined by Eq. (1).

$$\delta_\omega = \frac{\Delta V}{\frac{dV}{dy}_{max}} \tag{1}$$

Raynal [2] concluded from a linear stability analysis that the longitudinal wavelength λ_L can be expressed as in Eq. (2)

$$\lambda_L = C \delta_\omega \sqrt{\frac{\rho_l}{\rho_g}} \quad (2)$$

with a prefactor C close to 4. So far, experiments gave a somewhat lower prefactor. For a coaxial geometry, Mar-mottant [4] found C ranging between 1 and 1.7. For a planar mixing layer (i.e. in the experimental set-up previously used by Raynal), Ben Rayana et al. [5] established that C is also close to 1.6. The second mechanism in primary atomisation is due to the acceleration of the crest of the waves owing to the aerodynamic forces. According to Hong [6], this acceleration gives rise to Rayleigh–Taylor instabilities. These instabilities generate transverse waves leading to ligament formation (Fig. 1c). Hong [6] estimated the acceleration undergone by the crest of the wave as the ratio of the aerodynamic force on the liquid film to the liquid mass that is accelerated (Eq. (3)).

$$a = \frac{F}{m_n} = \frac{1}{2} \frac{C_d}{b} \frac{\rho_g}{\rho_l} (V_g - V_l)^2 \quad (3)$$

In this equation b (Eq. (4)) is the thickness of the longitudinal wave which is further supposed to be proportional to λ_L (Eq. (4)). V_c , is the convective velocity considered by Raynal.

$$b = B\lambda = BC\delta_\omega \sqrt{\frac{\rho_l}{\rho_l}}, \quad V_c = \frac{\sqrt{\rho_l}V_l + \sqrt{\rho_g}V_g}{\sqrt{\rho_l} + \sqrt{\rho_g}} \quad (4)$$

Hence, the wavelength of the transverse wave predicted by Hong [6], noted λ_T , becomes

$$\lambda_T = 2\pi \sqrt{\frac{6BC}{C_d}} \delta_\omega \left(\frac{\rho_l}{\rho_g}\right)^{1/4} \left(\frac{\rho_g(V_g - V_c)^2 \delta_\omega}{\sigma}\right)^{-1/2} \quad (5)$$

Raynal [2] obtained a dependence of δ_ω in $R_e^{-1/2}$. Considering that $V_g/V_l \gg 1$, Hong deduced, Eq. (6)

$$\lambda_T \propto V_g^{5/4} \quad (6)$$

Under the air stream action ligaments break-up in liquid cells (primary break-up) which are then atomized to small droplets (secondary break-up). Previous studies [4,6,7] show that the mean droplet diameter is proportional to the wavelength of transverse instabilities, so that the mean size is expected to evolve as $V_g^{5/4}$. Experiments [6] have indeed confirmed that behaviour since it was found that:

$$D_{32} \propto V_g^n, \quad 1.2 \leq n \leq 1.26 \quad (7)$$

For annular films in circular pipes, Azzopardi [8] obtained a correlation giving the droplet size issued from the film atomisation which depends on a Weber number.

$$D_{32} = \lambda_{Taylor} \frac{15.4}{\left(\frac{\rho_l}{\rho_g} We_{\lambda_{Taylor}}\right)^{0.58}} + 3.5 \frac{\dot{m}_{lE}}{\rho_l V_g} \quad (8)$$

In this expression, λ_{Taylor} is the Taylor scale ($= \sqrt{[\sigma/\rho_l g]}$) and \dot{m}_{lE} is the mass flux of droplet in the air flow by unit of surface. $We_{\lambda_{Taylor}}$ is a Weber number computed from the Taylor scale ($= [\rho_g V_g^2 \lambda_{Taylor}]/\sigma$). Hsiang and Faeth [9] classified the prediction a various secondary breakup regime based of experimental data a function of Ohnesorge Oh_d ($= \mu_l/[\sqrt{\rho_l \sigma} D_{32}]$) and Weber We_d ($= [\rho_g (V_g - V_l)^2 D_{32}]/\sigma$) numbers. This secondary break-up is limited to conditions where $Oh_d \leq 0.1$ and $We_d \leq 12$.

2.2. Faraday's instabilities – principle

Ultrasonic atomisation of liquids is currently used in a wide range of industrial and research applications. H.L. Berger [10] lists and describes a sampling of the more common applications of the ultrasonic technology. Earlier observations of a liquid film formed on a vibrating surface were obtained by Faraday in 1831 [11]. Since then, many studies were conducted to understand this mechanism and to find links between the excitation parameters, the development of standing waves at the free surface and the characteristics of resultant droplets [12]. Ultrasonic atomisation

resides in submitting a thin liquid film to a normal oscillation with adjustable ultrasonic frequency and amplitude. The liquid absorbs some of the vibratory energy, generating waves at the free surface of the film. Waves form a stationary rectangular grid in the liquid film with regularly alternating crests and troughs. This phenomenon is called Faraday's instabilities. When the resonance frequency is reached, the amplitude of oscillations grows until droplets are created from the crests. The main advantage of this atomisation process is its ability to generate a spray with a narrow distribution. In addition, as we shall see below, a control of the drop size is available by way of the frequency while an independent control of the flux is feasible from the acceleration.

2.3. Faraday's instabilities – theoretical and empirical knowledge

A few authors conducted theoretical studies to obtain laws predicting instabilities evolution or drop size distribution. On the basis of Kelvin and Rayleigh works on capillary waves and on sound theory, Lang [13] established Eq. (9) for the wavelength of Faraday capillary waves:

$$\lambda = \left(\frac{8\pi\sigma}{\rho f^2} \right)^{1/3} \quad (9)$$

Above some acceleration threshold, these waves form ligaments that break and produce droplets. The acceleration threshold proposed by Goodridge [14] is given by:

$$a_c = 3.03 \left(\frac{\sigma}{\rho} \right)^{1/3} f^{4/3} \quad (10)$$

Goodridge's equation (10) is based on experimental results with a constant liquid layer thickness equal to 10 cm. Baluteau [15] confirmed the exponent values obtained by Goodridge. However, Pyrtel [16] proposed another correlation where the effects of the liquid film thickness are taken into account.

$$a_c = k f^{16/9} h^{-2/3} \left(\frac{\sigma}{\rho} \right)^{1/9}, \quad k = 318.5 \times 10^{-6} \equiv [m^{4/3}] \quad (11)$$

Above this acceleration threshold, Lang (1962) related the droplet size to the wavelength through an empirical constant.

$$d_{30} = 0.34 \left(\frac{8\pi\sigma}{\rho f^2} \right)^{1/3} \quad (12)$$

Experimental investigation Sindayihebura [17] confirm Lang's results.

3. Experimental tools

3.1. Experimental set-up

Fig. 2 shows the downward vertical wind tunnel used for the experiments. It permits to obtain a uniform, symmetrical and non-turbulent air-stream at the outlet where the liquid injection system is fixed. Air stream is obtained from a high pressure tank. Two settling chambers linked together by four pipes allow to slow down the air velocity (Part I, Fig. 2a). The second settling chamber contains a screen followed by a honeycomb (Part II, Fig. 2a). The honeycomb, with its cells aligned in the flow direction, reduces the transverse velocity fluctuations while the woven-wire screens mainly reduces the streamwise velocity fluctuations. Finally a contraction (Part III, Fig. 2a) accelerates the air stream leading to a flat velocity profile at the outlet. The liquid is fed through two opposite intakes leading into a small tank. A slit 40 mm wide with a variable thickness (300 μ m and 1 mm) generates the wall liquid film representative of the prefilming zone of an injector (Fig. 2b). The air velocity ranged from 0 to 100 m/s and the water velocity from 0.4 to 2.32 m/s. Fig. 2b shows that the ultrasonic device couples a piezoelectric actuator and a mechanical amplification system. Two of them are tested. The first consists in a girder embedded on one side. The second corresponds to a sonotrode using compression wave. Each of these mechanical amplifiers have its own resonance frequency (1 kHz to 16 kHz for the girder and 35 kHz to 47 kHz for the sonotrode). The active surface of the girder or the sonotrode is flush mounted on the prefilming area so that the liquid film coming from the slit undergoes an acceleration normal to its interface. In order to analyse the influence of liquid properties, several solutions are used [2].

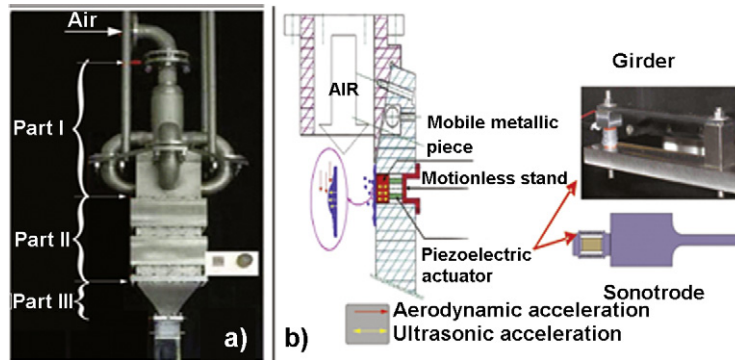


Fig. 2. (a) Wind tunnel with the film generator at the outlet. (b) Image of the injection system after modifications for the active method.

3.2. Technical measurement

LDA measurements: As shown in part 2.1, the air flow characteristics are determining factors in instabilities development. This is the reason why it is essential to define the air flow parameters and to measure its main characteristics. For this purpose, LDA measurements are carried out for three air velocities (10 m/s, 30 m/s and 100 m/s). The size of the measurement volume is equal to 90 μm in diameter and 1.3 mm in length. To make sure that the air stream is uniform in the flow core region before it shears the liquid film, the velocity distribution is measured in a first step for a complete section at the outlet of the contraction. In a second step, in order to determine the main characteristics of the air stream, detailed velocity profiles are carried out close to the wall along the x axis for different y positions just upstream of the liquid injection location. The accurate positioning of the measurement volume is ensured by the glass effect technique.

Visualisation: Front and side visualisations of the liquid film were carried out in order to study the behaviour of the liquid film and to determine the characteristic wavelength of instabilities observed at the liquid/air interface. A stroboscope synchronised with a CCD camera (25 Hz, 768×576 pixels) are used. The images are acquired on a PC board and post processed using the software IMAGE developed at ONERA. This software permits to perform different treatments on the image sequences in order to determine characteristic lengths linked to the interface instability.

Vibratory measurements: The velocity and the acceleration of the vibration imposed on the prefilming area by the actuator is measured with a Polytec optical vibrometer. This device detects the motion of solid surfaces using a non-intrusive interferometric technique and determines the velocity of the vibration. These measurements are used to determine the threshold level needed to atomise the liquid flowing on the wall.

Droplet size measurements: The size of the droplets issuing from the film atomisation, either from the air shearing effect or from the excitation action, are measured with a Malvern Spraytec system using light diffraction by the spray. Measurements are conducted at several positions [2], under different stream velocities and liquid film thickness. In order to ensure the accuracy of the measurement system, it is previously calibrated with monodispersed particles.

4. Results

4.1. LDA measurements

The boundary velocity profiles measured for the lower bulk velocities considered in this study (10 m/s and 30 m/s) are close to the Blasius law valid for laminar flows. For the higher bulk velocity used (100 m/s), although the velocity profile tends to a $1/7$ power law, the transition to turbulence is not fully reached. Whatever the conditions, the boundary layer thickness is approximately equal to 1 mm and the turbulence levels do not exceed 1% of the bulk velocity on the centre of the air stream. The vorticity thickness, which is a characteristic scale involved in the instabilities observed at the air/liquid interface, is found to be described by the following equation:

$$\delta_\omega = 3.56 \frac{H_g}{\sqrt{Re_{H_g}}} \quad (13)$$

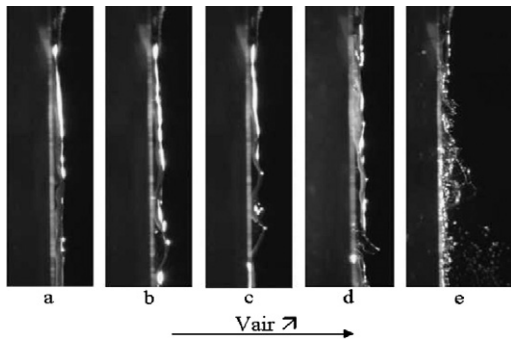


Fig. 3. Liquid behaviour according to V_g $h = 300 \mu\text{m}$, $V_l = 1 \text{ m/s}$; a: $V_g = 10 \text{ m/s}$, b: $V_g = 25 \text{ m/s}$, c: $V_g = 28 \text{ m/s}$, d: $V_g = 32 \text{ m/s}$, e: $V_g = 48 \text{ m/s}$.

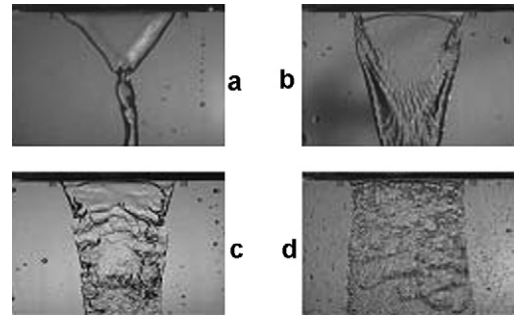


Fig. 4. Front visualisations of the liquid film $h = 300 \mu\text{m}$; a: $V_l = 0.2 \text{ m/s}$, $V_g = 0 \text{ m/s}$, b: $V_l = 1.4 \text{ m/s}$, $V_g = 0 \text{ m/s}$, c: $V_l = 0.7 \text{ m/s}$, $V_g = 30 \text{ m/s}$, d: $V_l = 0.7 \text{ m/s}$, $V_g = 80 \text{ m/s}$.

4.2. Qualitative film behavior

Fig. 3 depicts instantaneous side view images of $300 \mu\text{m}$ liquid film obtained for different air velocities. For air stream velocities lower than 20 m/s , a convergent film flows along the prefilming area (Fig. 3a), bounded by thick rims that are drawn together by surface tension (Fig. 4a). Increasing the liquid velocity, small distortions on the film surface appear which are indicative of the transition to turbulence (Fig. 4b). For air flow velocities between 20 m/s and 30 m/s , two kinds of longitudinal waves develop on the liquid/gas interface. At first, long rounded waves with small amplitude appear (Fig. 3b). When the air speed is increased, the amplitude of wave grows while their lengths diminish giving rise to triangular waves (Fig. 3c). When air velocity is further increased, disturbance waves are formed at the liquid surface as illustrated in Fig. 5d. Finally droplets formation occurs for higher air velocities (Fig. 3e). Front views of the liquid film before and after the beginning of the atomisation process are presented in Fig. 4c and Fig. 4d respectively. The key point here is that, compared with thick liquid layers [5], the onset of instability is delayed and the first droplets are observed for much larger air velocity, typically above 30 m/s (to be compared with $12\text{--}15 \text{ m/s}$ for thick liquid layers).

4.3. Characterization of wavelengths

Quantitative analyses are done to measure wavelengths of the longitudinal and transverse instabilities generated by aerodynamic forces at the gas/liquid interface. Optical properties of the liquid film in the front view configuration highlight the liquid film relief. Thus, concave areas which demarcate the wave appear dark while plane or convex areas, i.e. the crest of the waves, appear light. Image processing allows the measurement of the spacing between two dark lines. According to the camera resolution, the uncertainty on the wavelength determination lies between $2\%+$ and 4% . Automatic detection procedure is used over 50 images per liquid and gas flow conditions. Wavelengths are measured for each line or columns in single image, this operation is repeated afterwards for all 50 images. Averages values for wavelengths and the standard deviation ($\approx 0.175 \text{ mm}$) is obtained from the set of images. As shown by Fig. 5, the dependency of λ_L in δ_ω is linear, as in Raynal's model (Eq. (2)). However, our experimental values of λ_L are 10 times smaller than those obtained in previous works performed on thick liquid layers [5,6]. Indeed, in those works the liquid film was 10 mm thick while the present experiment it evolves between 0.3 and 1 mm . The thickness of the liquid film as well as the ratio between this thickness and the vorticity thickness may be influencing factors which will need to be taken into account. Fig. 6 illustrates experimental values of transverse wavelength with regards to V_g . The velocity dependence of λ_T is in good agreement with Hong's model. For $h = 1 \text{ mm}$, at gas velocities higher than 70 m/s , this evolution suffered attenuation: as expected, this behavior occurred as the wavelength becomes of the same order of magnitude than the film thickness.

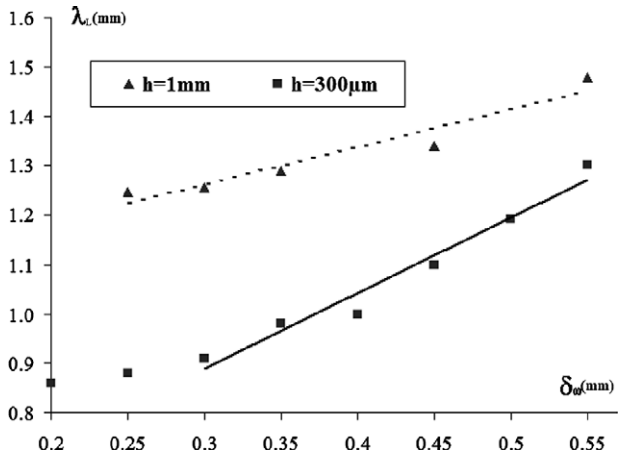


Fig. 5. Longitudinal wavelengths plotted with respect to δ_ω .

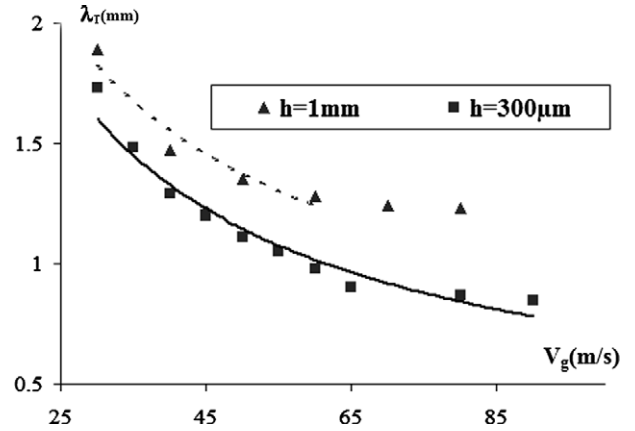


Fig. 6. Transverse wavelengths plotted with respect V_g .

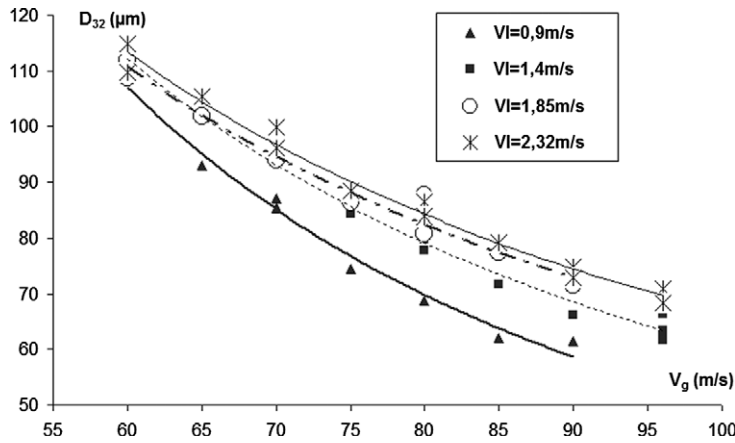


Fig. 7. D_{32} plotted with respect to V_g P_1 $h = 300 \mu\text{m}$.

4.4. Drop size measurements

Several positions, are chosen to analyze the evolution of drop sizes with respect to the distance from the wall and with the distance from the injection slit. Results indicate that there are no significant modifications in drop size whatever the position is, except for the position P_1 [2]. This result will be discussed later. Fig. 7 depicts for the position P_1 , the evolution of the Sauter mean diameter (D_{32}) for a fixed liquid velocity with respect to the velocity of the air stream.

Fitting curves using a power law are also plotted for each liquid velocity. It appears that the D_{32} decreases according to V_g^{-n} . Previous works indicate an exponent n ranging between -1.2 to -1.26 (cf. part 2.1). In the present experiments, the exponent n varies from -1.02 to -1.48 (see Fig. 9). Moreover, n increases as the liquid velocity decreases. Let us notice that the influence of the liquid velocity increases with the air velocities. This is confirmed when the D_{32} is plotted with respect to the liquid velocity for a fixed air velocity (Fig. 8). As before, a data fitting with a power law gives an exponent factor n ranged from 0.13 to 0.27 except for air velocity equal to 60 m/s for which n is equal to -0.0053 . This influence of the liquid velocity diminishes for location closer to the injection point. For a liquid film 1 mm thick, no influence of the measurement positions is observed. In parallel, we observe that when the liquid flowrate is augmented, the atomisation begins closer to the slit [2]. From these observations, it is supposed that a drying phenomenon occurs upstream of the P_1 location which diminishes the film thickness and consequently the droplet size. In Fig. 9 the variation of the D_{32} with air velocity for different liquid velocities measured for a liquid film 1 mm thick are plotted. In this case no influence of the liquid velocity is observed. Moreover, the exponent n ranges

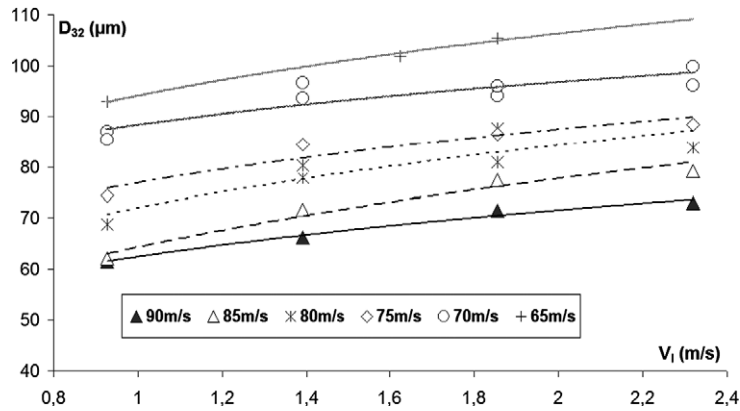


Fig. 8. D_{32} plotted with respect V_1 $P1$ $h = 300 \mu\text{m}$.

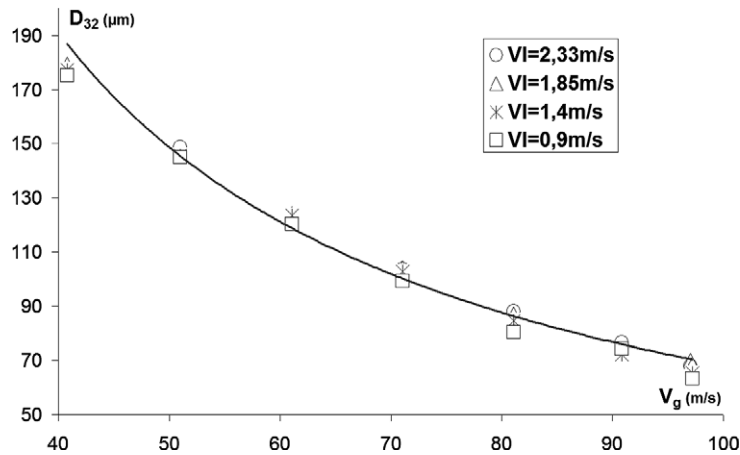


Fig. 9. D_{32} plotted with respect V_g $P1_{bis}$ $h = 1 \text{ mm}$.

from -1.12 to -1.18 , which remains consistent with model proposed by Hong [6] and by Varga [7]. At the condition of atomisation, the momentum flux ratio M ($= [\rho_g V_g^2] / [\rho_l V_l^2]$) is ranging between 0.4 and 16 and the Weber number We_d between 4.4 and $11.2 \leq 12$ (secondary breakup limiting).

The differences on the mean drop sizes measured at the same position but for two different film thicknesses (Figs. 7 and 9) show that the liquid film thickness has an influence. This is consistent with the observations made in Section 4.3 on the axial wavelength. This different behaviour can be due to the relative size of the boundary layer (or the vorticity scale) compared to the film thickness. Indeed, for $h = 1 \text{ mm}$, the condition $h \geq \delta_\omega$ is fulfilled for all the gas velocities considered and the expected behaviour obtained for thick film is recovered. This not the case for the other flow condition for which the film thickness is lower than the vorticity scale. The discrepancies obtained for the two film thicknesses investigated can be attributed to a modification of the effective axial acceleration undergone by the crest of the waves. Furthermore, a limitation in the wave amplitude due to the proximity of the bottom wall can be expected. To quantify these effects, more experiments are needed to span a wider range of flow conditions. Finally, it must be noticed that for the two film thicknesses investigated, the resultant droplets are larger than $100 \mu\text{m}$ for air velocities below 70 m/s . Such sizes are not favourable for an efficient combustion.

4.5. Ultrasonic excitation of the liquid film

The following chapter presents the first results and visualisations of the disintegration of a liquid film by ultrasonic atomisation. At the resonance frequency, which depends on the geometrical characteristics of the mechanical system, the direction of vibration is strictly perpendicular to the atomizing surface. When the amplitude of the excitation

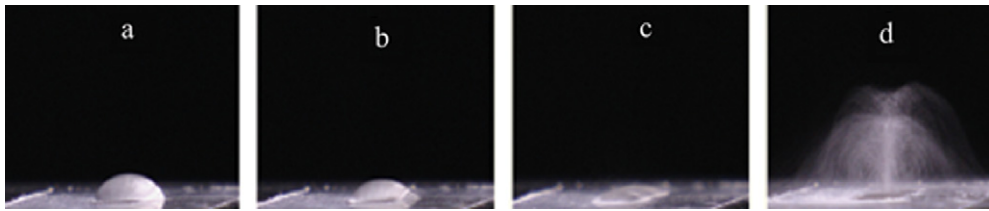


Fig. 10. Visualisation steps of the pulverisation a liquid due to instabilities $f = 35 \text{ kHz}$, $h < 1 \text{ mm}$ (a: $U = 0 \text{ V}$, b: $U = 3.0 \text{ V}$, c: $U = 8.5 \text{ V}$ and d: $U = 13.5 \text{ V}$).

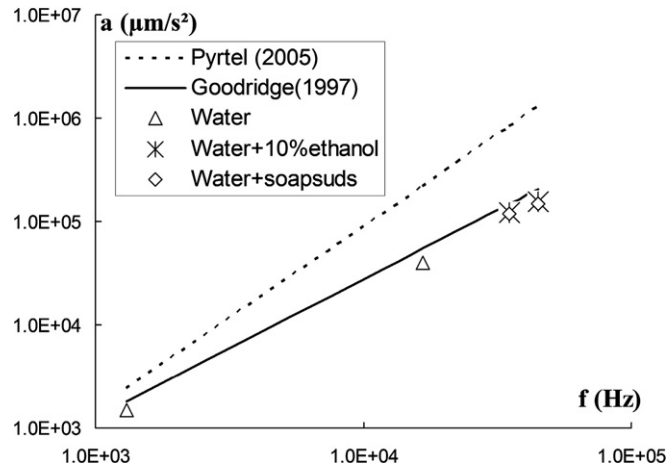


Fig. 11. Threshold acceleration as a function of the excitation frequency.

Table 1
Summary of experimental conditions.

	Frequency range	Film thickness
Goodridge (1997)	20–80 Hz	10 cm
Pyrtel (2003)	100–650 Hz	1–6 mm
Present work	1–45 kHz	$\leq 1 \text{ mm}$

is increased, the amplitude of the capillary waves augments accordingly. Finally, tiny drops of liquid are ejected when the applied amplitude exceeds a threshold value. As an example of the droplet atomisation on the oscillating surface, photographs of the atomisation phenomena of water are shown in Fig. 10. Images illustrate the case of a motionless liquid film lying on a horizontal plate. When the resonant frequency of the mechanical system is reached and the amplitude of excitation increases, the drop flattens and Faraday’s instabilities appear on the interface (Fig. 10, images b–c). Once the displacement threshold is reached, break-up of ligaments and the formation of droplets start (Fig. 10, image c). When the amplitude of excitation is further increased, the ultrasonic atomisation becomes more powerful and the initial liquid film is completely pulverized (Fig. 10, image d). Experiments are also conducted with droplets of the some liquid dropping on a vertical mechanical system submitted to ultrasonic oscillation. When hitting the active surface they are atomized into a spray of droplets.

4.5.1. Displacement threshold measurements

In Fig. 11 the threshold acceleration needed to atomise the liquid is plotted with respect to the excitation frequency. The results obtained in our study are consistent with the extrapolation of the Goodridge and Baluteau correlations [14,15] to the frequencies used in this work. This is not the case of the extrapolation of the Pyrtel’s correlation which greatly overestimates the acceleration threshold needed even if his thickness and frequency parameters are closer to our condition (Table 1). This contradiction is the subject of an ongoing investigation.

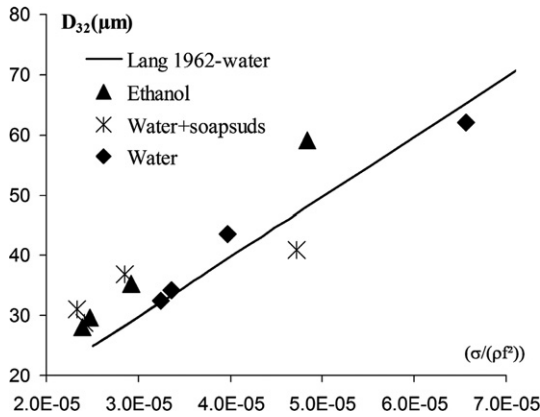


Fig. 12. Effects of the liquid properties and the excitation frequency on the D_{32} .

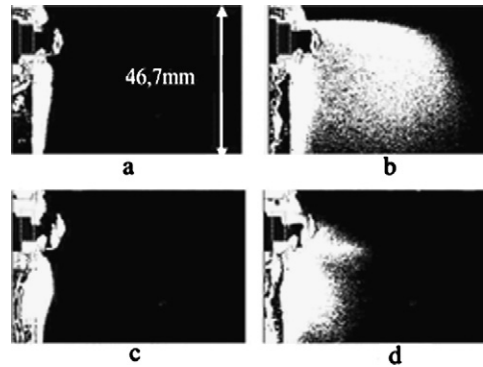


Fig. 13. Illustrations of the combined effects of shearing instabilities – Faraday’s instabilities on the spray penetration (cf. Table 2: experimental conditions).

Table 2
Summary of experimental conditions.

Image	V_g (m/s)	f (kHz)	U (mV)
a	0	0	0
b	0	14.7	90
b	10	0	0
a	0	14.3	90

4.5.2. Drop size distributions

Ultrasonic sprays are characterized by a narrow, nearly monodisperse distribution compared to those produced by classical atomizers. Surface waves theory in ultrasonic atomisation is based on the hypothesis that the droplets are emitted from the crests of the unstable surface waves.

Influence of frequency: The effects of working frequency on the Sauter mean diameter (D_{32}) has been studied by several authors (Lang [13], Sindayihebura [17]). Fig. 12 compares Lang’s correlation to our experimental results. The experimental result confirms the results found in the literature. When the excitation frequency is set to 50 kHz, the droplet diameter is approximately equal to 23 μm . Such sizes are favourable for an efficient combustion.

Influence of the liquid properties: Our experimental study involved viscosity, surface tension and density. The influence of each parameter is analyzed as well as the interaction between these effects. Fig. 12 illustrates the variation of the D_{32} over the excitation frequency for multiple liquids. The linear dependency of $[\sigma/(\rho f^2)]^{1/3}$ is well fitted by Lang’s correlation.

Fig. 13 presents visualisations of the spray obtained for different flow conditions. The image (a) shows the envelope of the film without air flow and excitation but with a liquid flow rate ($V_l = 0.9$ m/s). When the acceleration increases above the atomisation threshold, the spray penetration is enhanced (image 13(b)). The images 13(c) and (d) are obtained with a 10 m/s vertical downward air flow without and with excitation respectively. When the actuator is switch off, no atomisation is obtained from the film. When the actuator is switch on, a spray is produced that still penetrates the strong gas flow. The depth of penetration is somewhat lower compared with the zero gas velocity case because of the entrainment of the small droplets by the gas stream. These results validate the feasibility of the proposed active method on the prefilming area of an air assisted injector.

In Fig. 14 the droplet size distributions obtained without excitation (a) and with excitation (b) for a gas velocity of 60 m/s are shown. The influence of the excitation is evident on this graph. The graph (b) shows that the two mechanisms of atomisation can coexist influencing the size distribution. Between the two cases, the Sauter mean diameter D_{32} is reduced by 20%.

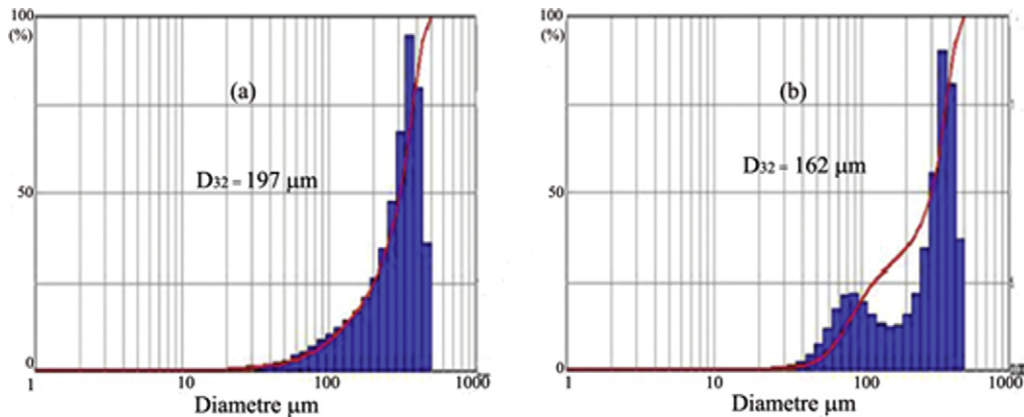


Fig. 14. Effect of the active methods on the volume droplet size distribution $V_g = 60$ m/s, $h_l = 300$ μm , $V_l = 0.9$ m/s; (a) without excitation; (b) with excitation $f = 15.4$ kHz, $U = 140$ mV.

5. Conclusion

The aim of this study is to investigate the atomisation of a liquid film by a parallel air flow and the consequences of an active method applied to the liquid phase. In that scope an experimental setup is built and the air flow is characterised. The results gathered so far indicate that, for the air assisted atomisation of a thin film, the wavelengths and the drop size dependencies with the air flow characteristics are in agreement with previous investigations performed with thick liquid layers. Nevertheless, for liquid films thinner than the vorticity thickness of the surrounding gas flow, some deviations in the results appear. In this case, the film thickness becomes one parameter of the problem which must be taken into account in the models. Such a situation, apparently not referenced in the literature, deserves to be more thoroughly investigated. The break-up of a thin liquid film due to aerodynamic forces is characterized and it is shown that the droplet sizes obtained for low air velocities are somewhat too large for combustion purposes. In order to diminish the mean drop size, it is proposed to combine the shear instability with an active method based on Faraday instabilities. The performances of such a system combined with air assisted atomisation are investigated. The drop size due to Faraday instabilities is found to follow Lang's correlation over the whole range of conditions considered, indicating that the forcing frequency controls the drop size. The acceleration threshold at the onset of atomisation is determined and is found consistent with previous studies. Such a result is a good indication that the drop flux can be controlled by the acceleration amplitude, and so by the voltage applied on the piezo electric actuator. Finally, the actuator is proved efficient both on moving liquid films and in presence of a strong co-flowing gas stream. Thus, the technique is potentially suitable to control the drop size and the flux in air assisted injection devices. Progress are however necessary to quantify the flux of droplets as a function of the control parameters and aerodynamic conditions. Another step would be to extend the investigation to an axisymmetric geometry.

Acknowledgements

This study was carried out as part of a DGA PhD (Marie Lalo) and a SNECMA PhD (Madjid Boukra). It was support by a DPAC program and SNECMA contract.

References

- [1] C. Dumouchel, On the experimental investigation on primary atomization of liquid streams, *Experiment in Fluids* 45 (3) (2008) 371–422.
- [2] M. Lalo, Atomisation d'un film liquide mince par action combinée des instabilités de Kelvin–Helmholtz et de Faraday. Application aux injecteurs aérodynamiques des turbomachines aéronautiques, Ph.D. thesis, ENSAE, 2006.
- [3] L. Raynal, Instabilité et entraînement à l'interface d'une couche de mélange liquide-gaz, Ph.D. thesis, Laboratoire des écoulements géophysiques et industriels, 1997.
- [4] P. Marmottant, Atomisation d'un liquide par un courant gazeux, Ph.D. thesis, Laboratoire des écoulements géophysiques et industriels, 2001.
- [5] F. Ben Rayana, A. Cartellier, E. Hopfinger, Atomisation primaire en injection diphasique assistée : rôle de la géométrie, in: 17^{ème} Congrès Français de Mécanique, 2005.

- [6] M. Hong, Atomisation et mélange dans les jets coaxiaux liquide-gaz, Ph.D. thesis, Laboratoire des écoulements géophysiques et industriels, 2003.
- [7] C. Varga, Initial breakup of a small diameter liquid jet by a high speed gas stream, Ph.D. thesis USCD, San Diego, 2002.
- [8] B.J. Azzopardi, Drops in annular two phase flow, *International Journal Multiphase Flow* 23 (Suppl.) (1997) 1–53.
- [9] L.P. Hsiang, G.M. Faeth, Near limit drop deformation and secondary breakup, *International Journal Multiphase Flow* 18 (5) (1992) 635–652.
- [10] H.L. Berger, *Ultrasonic Liquid Atomization, Theory and Application*, Partridge Hill Publishers, 1998.
- [11] M. Faraday, On the forms and states assumed by fluids in contact with vibrating elastic surfaces, *Philosophical Transactions of the Royal Society of London* 52 (1831) 319–340.
- [12] N. Bremond, C. Clanet, E. Villermaux, Atomization of undulating liquid sheets, *Journal of Fluid Mechanics* 585 (2007).
- [13] R.J. Lang, Ultrasonic atomization of liquids, *The Journal of the Acoustical Society of America* 34 (1) (1962) 6–8.
- [14] C. Goodridge, Viscous effects in droplet ejecting capillary waves, *Physical Review E* 56 (1) (1997) 472–475.
- [15] M. Baluteau, Production de gouttes par accélération harmonique d'une surface libre : seuil critique et distributions de tailles, DEA, LEGI, 2001.
- [16] F. Pyrtel, Vibration induced generation from a liquid layer for evaporative cooling in a heat transfer cell, Ph.D. thesis, Georgia Institute of Technology, 2005.
- [17] D. Sindayihebura, Pulvérisation ultrasonique des films liquides de faible épaisseur, Ph.D. thesis, Université Catholique de Louvain, 1995.